Effect of Early Age Strength on Cracking in Mass Concrete Containing Different Supplementary Cementitious Materials: Experimental and Finite-Element Investigation

Adrian M. Lawrence, A.M.ASCE[1]; Mang Tia[2]; Christopher C. Ferraro[3]; and Michael Bergin[4]

Abstract: This paper presents the findings of an investigation using the finite-element method to predict the distribution of temperatures within a hydrating massive concrete element. The temperature distribution produced by the finite-element thermal analysis of the model is used in the finite-element structural analysis to quantify the maximum allowable internal temperature difference before cracking will initiate in the concrete. To verify the results obtained in the finite-element model, four different mixes of concrete, typical for use in mass concrete applications in Florida, were produced and each mix was used to make two large-scale 1.07 m × 1.07 m × 1.07 m (3.5 ft × 3.5 ft × 3.5 ft) concrete blocks. The mechanical and thermal properties of early age concrete used values obtained experimentally from the concrete used to construct the four sets of blocks. The temperature distributions produced by the model were shown to be very similar to those measured in the experimental blocks. Results suggest that reliance on a limiting maximum temperature differential to control cracking in massive concrete applications should be supplemented with a requirement for the presentation of an analysis showing the calculated stress response to the predicted temperature distribution within the concrete to ensure that the induced tensile stresses will not exceed the tensile strength of the concrete. **DOI: 10.1061/(ASCE)MT.1943-5533.0000389.**

CE Database subject headings: Concrete; Cement; Temperature effects; Thermal stress; Finite element method; Aging (material).

Author keywords: Mass concrete; Supplementary cementitious materials; Temperature differential; Thermal stresses; Finite element; Early age strength.

Introduction

Whenever fresh concrete is used in the construction of large homogeneous structures, such as foundations and dams, consideration is always given to the amount of heat that will be generated and the resulting volume change. Volume changes occur because of temperature changes in the structure that initially increase as the concrete hydrates and decrease as the reaction is exhausted. Temperature difference per unit distance between one point and another in a structure is called a thermal gradient. Temperature gradients are produced when the heat being generated in the concrete is dissipated to the surrounding environment, causing the temperature at the surface of the concrete to be lower than the temperature at the interior of the concrete. This temperature drop at the surface results in the contraction of the concrete. With the interior of the concrete being more mature than the surface, it acts as a restraint against the contraction, creating tensile stresses in the surface. Given the time window concerned in the study of early age mass concrete, drying shrinkage is negligible and autogenous shrinkage is not considered, which is consistent with American Concrete Institute (ACI) 207.2R.

The magnitude of the tensile stress is dependent on the thermal differential in the mass concrete, the coefficient of thermal expansion, modulus of elasticity, creep or relaxation of the concrete, and the degree of restraint in the concrete. Because the concrete is still in its early age, its full tensile strength is not developed, and if the tensile stresses are larger than the early age tensile strength, cracking will occur (ACI 207.1R; ACI 207.2R). If cracking does occur, it will ultimately affect the ability of the concrete to withstand its design load and allow the infiltration of deleterious materials that undermine durability.

The behavior of concrete at an early age is influenced by the heat generated, which, by extension, dictates the temperature distribution during hydration. The temperature profile of a concrete element is further affected by the specific heat capacity, thermal diffusivity, and emissivity of the concrete. At the same time, the rate of development of mechanical strength of concretes at an early age increases with increasing temperature and, hence, can be expressed as a function of temperature and time.

Past research leading to the creation of numerical models for the prediction of temperature distribution in mass concrete has primarily focused on using generic heat generation functions for the calculation of adiabatic temperature rise. The use of actual measured heat from hydration results of calorimetry testing of the concrete paste has been mostly neglected. At the same time, attempts at modeling hydrating mass concrete have treated the heat generated by the reacting cement as being uniform throughout the concrete

[1]Post-Doctoral Associate, Dept. of Civil and Coastal Engineering, Univ. of Florida, P.O. Box 116580, 365 Weil Hall, Gainesville, FL 32611 (corresponding author). E-mail: alawrence@ce.ufl.edu

[2]Professor and Associate Chair, Dept. of Civil and Coastal Engineering, Univ. of Florida, P.O. Box 116580, 365 Weil Hall, Gainesville, FL 32611. E-mail: tia@ce.ufl.edu

[3]Assistant in Engineering, Dept. of Civil and Coastal Engineering, Univ. of Florida, P.O. Box 116580, 365 Weil Hall, Gainesville, FL 32611. E-mail: ferraro@ce.ufl.edu

[4]State Structural Materials Engineer, Florida Dept. of Transportation, State Materials Office, 5007 NE 39th Ave., Gainesville, FL 32608. E-mail: michael.bergin@dot.state.fl.us

Note. This manuscript was submitted on October 1, 2010; approved on September 14, 2011; published online on September 16, 2011. Discussion period open until September 1, 2012; separate discussions must be submitted for individual papers. This paper is part of the ***Journal of Materials in Civil Engineering***, Vol. 24, No. 4, April 1, 2012. ©ASCE, ISSN 0899-1561/2012/4-362–372/$25.00.

Table 1. Mix Designs of Concrete Used in Large-scale Blocks

Material	Mixture 1100% Portland cement (kg/m^3)	Mixture 250% Portland-50% slag (kg/m^3)	Mixture 365% Portland-35% fly ash (kg/m^3)	Mixture 450% Portland-30% Slag-20% fly ash (kg/m^3)
Cement	236	118	153	118
GGBF Slag	0	118	0	71
Fly Ash	0	0	83	47
Water	118	118	118	118
Fine Agg.	380	377	359	364
Course Agg.	564	580	576	572

mass (Radovanovic 1998), whereas, in reality, the heat generation is a function of the temperature and time history of the concrete at individual locations in the concrete mass. Different locations in a mass concrete element have different time-temperature conditions. Studies have also been conducted to create a step-by-step approach that can correctly simulate the stress history of maturing concrete with varying internal temperatures, to improve the stress modeling within commercial finite-element software (Ayotte et al. 1997).

This study (Tia et al. 2009) was aimed at formulating a finite-element model, taking into consideration the nonhomogeneity of heat generation within concrete, to accurately predict the distribution of temperature in a hydrating concrete mass, the resulting thermal gradients, and associated thermal stresses and strains. Knowledge of these phenomena will allow for a reasonably accurate prediction of the location and potential for cracking of concrete.

Research Significance

The high amount of heat that develops during the hydration of massive concrete structures produces very high temperatures throughout the structure. The variation in the rate of heat production at different locations within the concrete (Ballim 2004) results in temperature gradients that have the potential to cause microcracking as some sections cool down toward ambient temperature whereas others are still being heated. Although the effects that thermal gradients have on concrete is well known, no agreement exists on what the maximum allowable temperature differential between the center of a mass concrete element and its surface to prevent thermal cracking should be. The Florida Department of Transportation (FDOT) allows a maximum temperature differential of 20°C (or 35°F) between the core temperature and the exterior surface of the concrete element as measured by

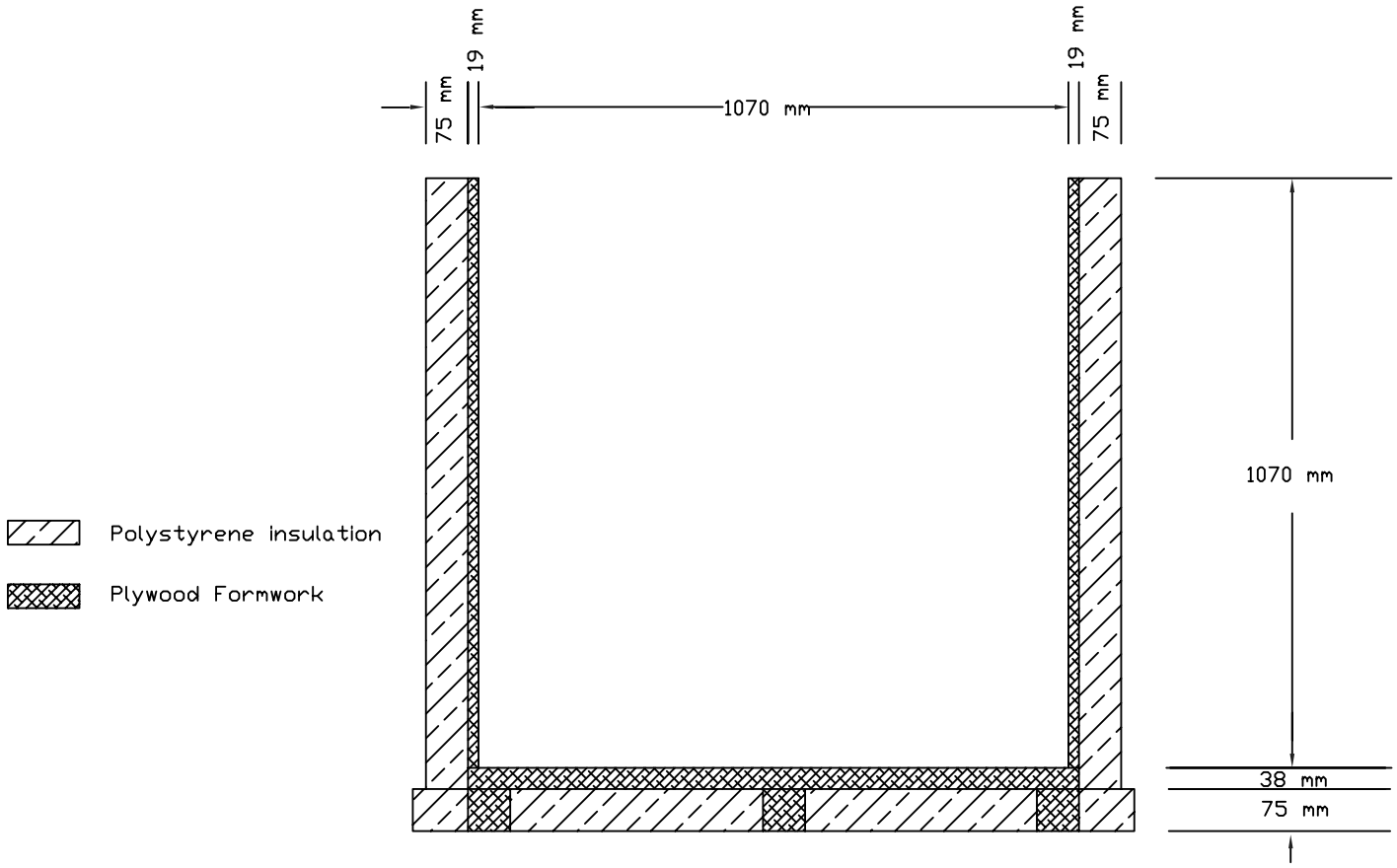

Fig. 1. Experimental block geometry

J. Mater. Civ. Eng., 2012, 24(4): 362-372

Fig. 2. Uninsulated (left) and insulated (right) mass concrete block specimens (image by Adrian M. Lawrence)

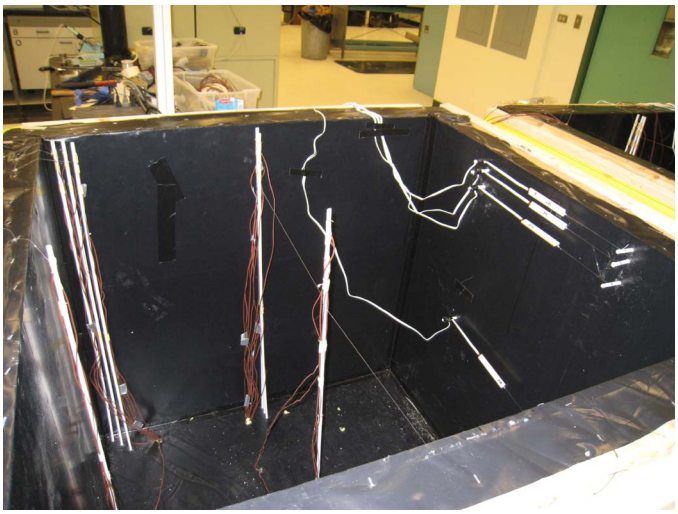

Fig. 3. Instrumentation layout for experimental block (image by Adrian M. Lawrence)

temperature sensors (FDOT 2007). In Colorado, the specifications state that the temperature differential between the midpoint and a point 50 mm (2 inches) inside the exposed face of all mass concrete elements shall not exceed 25°C (or 45°F) as measured between temperature sensors. ACI 207.2R also recommends a maximum temperature differential of 20°C (or 35°F). The results of this study show that cracking in mass concrete is more dependent on the attained early age strength than the magnitude of the temperature differential.

Experimental and Modeling Procedures

The finite-element analysis utilized Displacement Analyzer's (DIANA) staggered flow-stress analysis' feature, in which the thermal analysis is combined with a subsequent structural analysis (DIANA Version 9.3). The model comprised two domains: one for the thermal flow analysis and one for the structural analysis. The concrete is active in the flow-stress domain and calls for modeling with the use of a structural element. For this, we selected a

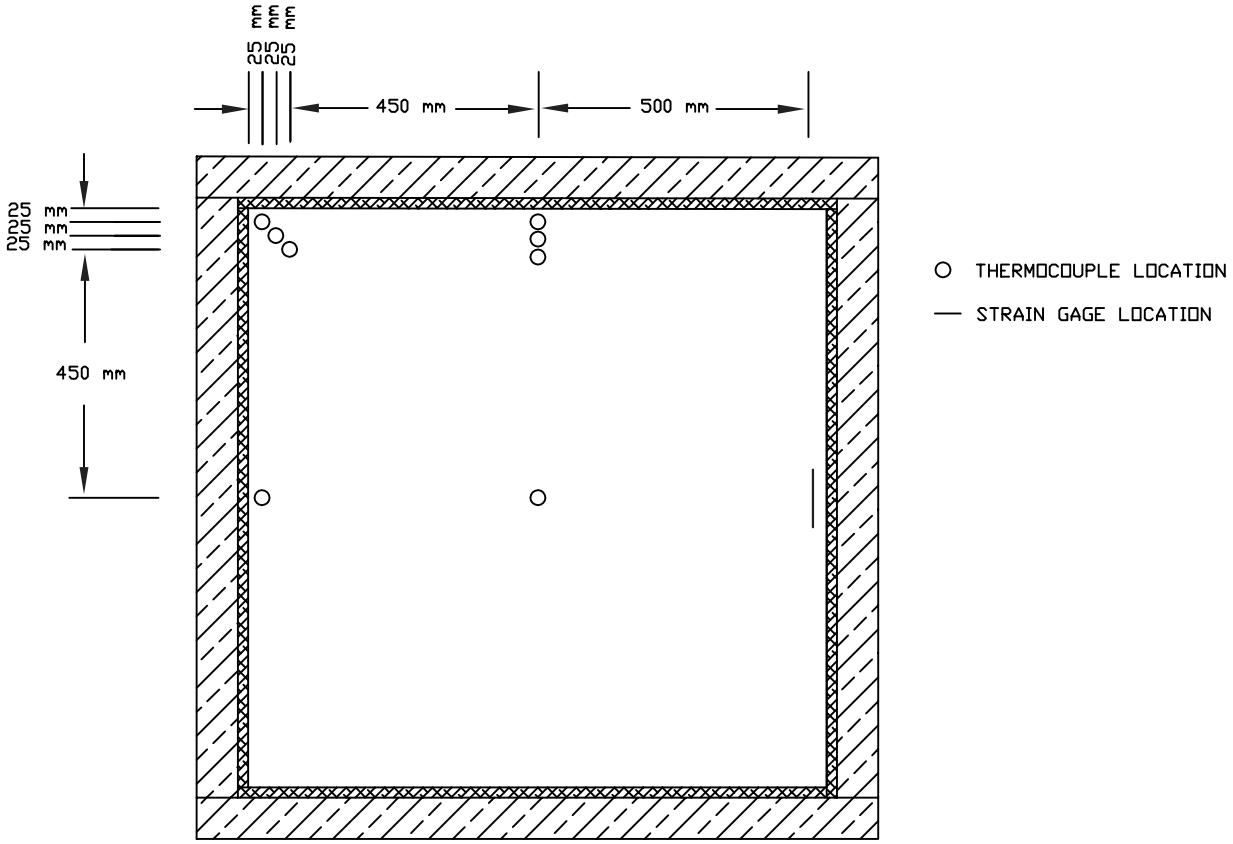

Fig. 4. Thermocouple location (plan)

J. Mater. Civ. Eng., 2012, 24(4): 362-372

three-dimensional twenty-node structural brick element that is converted to a three-dimensional eight-node isoparametric brick element for the thermal analysis. Both types of elements have coinciding corner nodes. However, because the structural element is quadratically interpolated and the thermal element is linearly interpolated, the midnodes of the structural element are disregarded in the thermal analysis.

To verify that the finite-element model created was effective in modeling early age behavior of hydrating mass concrete, four different mixes of concrete, typical of use in mass concrete applications in Florida, were produced. Each mixture was used to make large concrete blocks with dimensions that qualify them to be characterized as massive concrete elements. All of the four concrete mixes used in this study had a water to cementitious material ratio of 0.5 to allow for compatibility with isothermal calorimetry testing that was used to determine the activation energies and heat of hydration (per ASTM C 1702) of each concrete mix. Measurements of the temperature and strain at predetermined locations within the blocks were recorded until the equilibrium temperature was achieved. The locations were chosen on the basis of Section 346–3.3 of the Florida Department of Transportation Standard Specifications for Road and Bridge Construction, which states that the temperature development between the core center and a point two inches within the exterior surface (s) of mass concrete elements must be monitored.

Mix 1, a control mix, consisted of 100% Type I Portland cement concrete; Mix 2 had 50% of the Portland cement mass replaced by ground granulated blast-furnace slag; Mix 3 contained 65% Portland cement and 35% Class F fly ash; and Mix 4 was a blend of 50% Portland cement, 30% granulated blast-furnace slag, and 20% Class F fly ash. The mix designs for each block are shown in Table 1. The coarse and fine aggregates were adjusted according to the volumetric differences caused by the varying densities of each cementitious material.

Two 1.07 m × 1.07 m × 1.07 m forms were created for placing of the experimental concrete blocks. The geometry of the blocks is presented in Fig. 1. The side faces and base of both blocks consisted of a 19 mm thick plywood formwork surrounded by a three-inch thick layer of polystyrene plates. However, one of the blocks had a cover with the same make-up as the sides placed on its top surface after placing was completed in an effort to simulate a fully adiabatic process, whereas the top face of the other block was left open and exposed to environmental conditions. Fig. 2 is a photograph of the two blocks after the concrete was placed.

The two concrete blocks were instrumented for the monitoring of early age temperatures and strain at predetermined locations. The data acquisition equipment consisted of Type *K* thermocouples with an accuracy of ±0.5°C and embedded strain gauges.

The layout of the thermocouples and strain gauges are presented in Figs. 3–5. The thermocouples were mounted onto fiberglass rods that had the same thermal properties of the concrete being placed, allowing for accurate temperature readings. The thermocouple data and the strain data were recorded to validate the finite-element model's ability to accurately predict the early age behavior of the concrete block specimens.

The location of the thermocouples in the blocks were chosen to capture the temperature difference between the center of the block

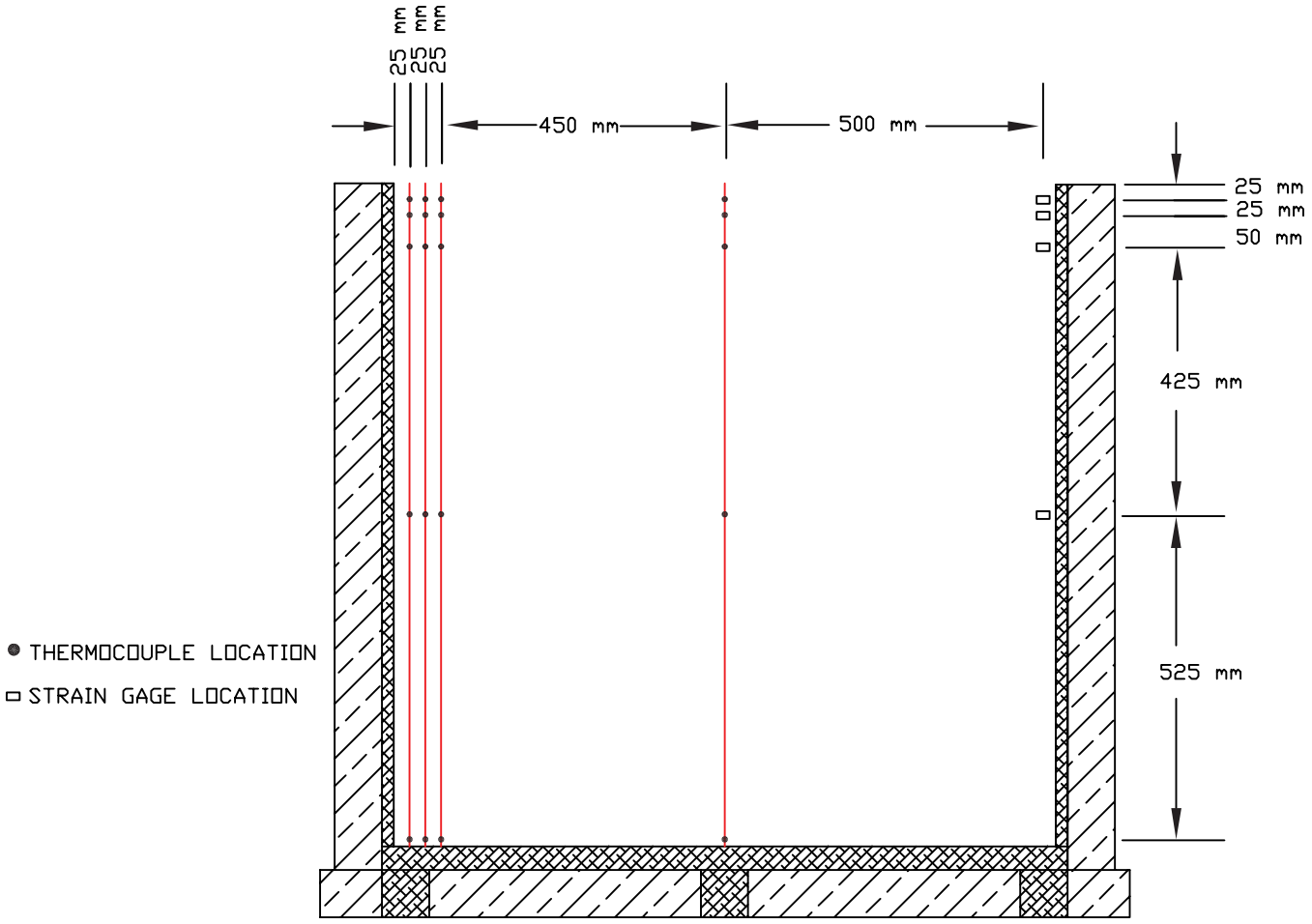

Fig. 5. Thermocouple location (section)

J. Mater. Civ. Eng., 2012, 24(4): 362-372

and the exposed surface, and to monitor the near surface temperature gradient to determine if it would contribute to thermal cracking of the concrete. The thermocouples at the sides and bottom of the block were placed to validate the effectiveness of the insulation and by extension the thermal boundary conditions that would be used in the finite-element model.

Results

The determination of the heat generated during the hydration of the concrete is essential for the characterization of its thermal behavior at early ages. One of the experimental methods in use today, isothermal calorimetry testing (Evju 2003), was utilized in this research. Isothermal conduction calorimetry is a very useful testing method for the determination of the heat energy evolved from the hydration of a cementitious material over time. It provides a direct measurement of the heat generated by a relatively small specimen, avoiding the errors associated with methods that utilize chemical analyses. For this study, 6 g samples of the cementitious materials used in each of the experimental blocks were used. The specimens were tested at temperatures of 15°C, 23°C, 38°C, and 49° C, using a Tam-Air isothermal calorimeter. The data curves produced by the test at each temperature were analyzed for the energy rise versus time. The curves were then converted to energy rise with respect to equivalent age that showed that, regardless of the test temperature, the energy rise of the cement pastes were virtually equal, with the exception of the testing that occurred at 15°C. Ferraro (2009) found that the heat rise for the same cement tested at a lower isothermal temperature may give rise to a higher energy for a given equivalent age. For the use in this work, the relationship for temperatures above 15°C as presented in Fig. 6 was used to obtain the relationship between energy rise and temperature rise, which could then be used in the input for the finite-element model.

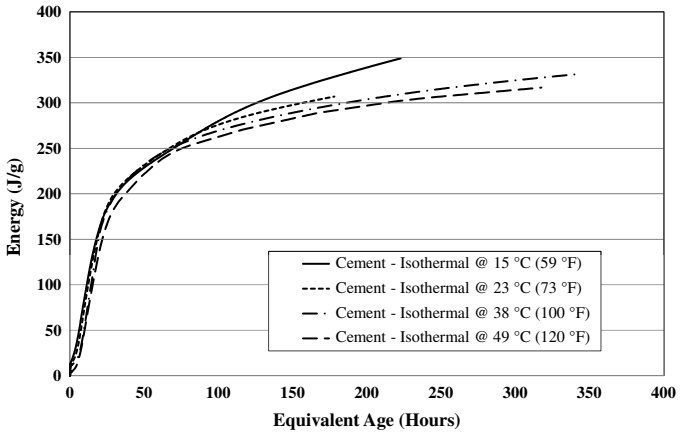

Fig. 6. Resultant isothermal calorimetric curves with regard to energy versus equivalent age for mix 1

Table 2. Thermal Properties of Concrete

	Conductivity (J/m − hr − °C)	Heat capacity (J/m3 − °C)	Activation energy (J/mol)
Mixture 1	7920	2675596	34235
Mixture 2	4418	2017434	50400
Mixture 3	5883	2603101	32982
Mixture 4	4838	2024985	37330

Table 3. Thermal Properties of Plywood and Polystyrene

	Conductivity (J/m − hr − °C)	Heat capacity (J/m^3 − °C)
Plywood	540	85440
Polystyrene	224.85	20824

The other properties necessary to model the thermal behavior of the concrete blocks were measured experimentally and include the activation energy, the specific heat, and the thermal conductivity (which was derived from diffusivity testing on cylinders made from sampling the concrete used in each block mixture). The values obtained are presented in Table 2. The conductivity and heat capacity values of the polystyrene foam shown in Table 3 were obtained from the manufacturer's specifications, whereas for the plywood, the typical conductivity and specific heat capacities for plywood used in North America were used. In this study, a constant convection coefficient value (Faria 2006) of 5.6 W/m^2 − °C or 20106 J/m^2 − hr − °C was used for all analyses because all experimentation was conducted in a temperature-controlled laboratory environment maintained at a constant temperature of 20 ± 2°C with negligible forced air flow.

Modulus of Elasticity and Poisson's Ratio Testing

To correctly model the thermal stresses in young concrete, including the variation of the mechanical properties with time was essential (De Schutter 2002), most importantly the elastic modulus. Testing for both the compressive and tensile moduli of elasticity was conducted.

The compressive modulus of elasticity and Poisson's ratio of concrete was determined using the ASTM C469 standard test method. The stress-strain relationship obtained from the middle third section of the 150 mm × 150 mm × 550 mm beams tested using the ASTM C78 third point bending test with a strain gauge attached to the top and bottom was used to calculate the tensile modulus of elasticity of the respective concrete mixtures. This was done because cracking in mass concrete is primarily a phenomenon of tensile action, also the failure mode of the flexural test beams. The results of the modulus of elasticity testing are presented in Figs. 7 and 8. The compressive modulus was found to be the higher of the two types of modulus of elasticity and therefore used in the finite-element analysis because it was the more conservative description of the stress-strain relationship of the concrete. The values are presented in Table 4.

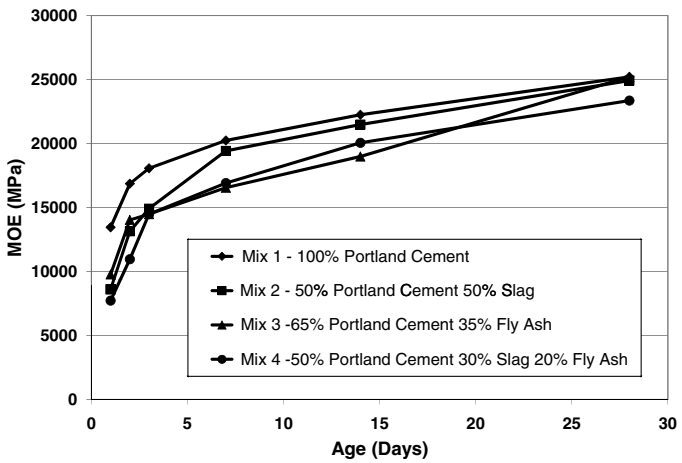

Fig. 7. Compressive modulus of elasticity versus time

J. Mater. Civ. Eng., 2012, 24(4): 362-372

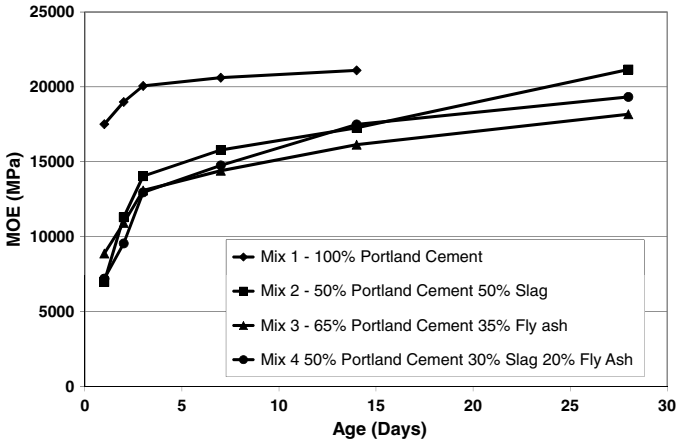

Fig. 8. Tensile modulus of elasticity versus time

Splitting Tensile Strength

The splitting tensile strength test was performed on 100 mm × 200 mm cylinders specimens, sampled from each concrete mixture, in accordance with ASTM C496. The tests were carried out at ages 1, 2, 3, 7, 14, and 28 days and are presented in Table 4, and the strength development over time of the concrete of each mix is observed.

Coefficient of Thermal Expansion Testing

The results of testing for the coefficient of thermal expansion of the concrete mixtures used in this research are shown in Table 5. The testing was performed in accordance with AASHTO T 336 by placing 100 mm × 200 mm cylinder specimens in a measuring apparatus consisting of LVDTs located in a temperature-controlled bath. The specimens were allowed to attain thermal equilibrium with the bath before commencing the test.

As shown in Fig. 9, very little change (less than 5%) occurred in the values for each mix over the first seven days, which was the duration of the analysis of the finite-element model. Therefore, a constant input value for the coefficient of thermal expansion of each model block was decided to be sufficient for the analysis.

Table 4. Mechanical Properties of Concrete

	Time (Days)	Compressive strength (MPa)	Modulus of elasticity (MPa)	Tensile strength (MPa)
Block 1	1	10.60	13445	1.25
(100%	2	14.87	16892	1.66
Portland	3	17.70	18064	1.93
cement)	7	24.32	20236	2.206
	14	27.46	22248	2.972
	28	32.47	25213	3.303
Block 2	1	1.95	8618	0.255
(50% Portland	2	5.93	13170	0.807
50% slag)	3	9.40	14893	1.23
	7	17.53	19443	2.31
	14	23.58	21481	2.45
	28	31.11	24921	2.99
Block 3	1	4.96	9791	0.669
(65% Portland	2	7.29	13996	0.931
35% fly ash)	3	9.58	14479	1.28
	7	12.46	16547	1.63
	14	15.84	18985	1.91
	28	32.47	25235	3.30
Block 4	1	2.05	7722	0.393
(50% Portland	2	5.98	10963	0.765
30% slag	3	8.36	14479	1.01
20% fly ash)	7	15.56	16905	1.82
	14	21.86	20053	2.20
	28	28.11	23352	2.85

Table 5. Poisson's Ratio and Coefficient of Thermal Expansion of Concrete

	Poisson's ratio	Coefficient of thermal expansion (mm/mm − °C)
Block 1	0.19	9.16E-06
Block 2	0.20	1.11E-05
Block 3	0.20	1.11E-05
Block 4	0.20	1.004E-05

Model Geometry

Fig. 10 shows the model depicting the concrete exposed to ambient conditions at the top surface and with the plywood and polystyrene insulation at the bottom and sides. To improve the efficiency of the analysis, advantage was taken of the double symmetry of the block, which allowed for the modeling of one-quarter of the block. The vertical height of the block, extends in the z direction, and the width and length extend in the x and y directions, respectively. The polystyrene insulation, plywood, and concrete were explicitly discretized and modeled according to their corresponding thermal properties.

Finite-Element Analysis

The thermal analysis utilizes linear interpolation and Gauss integration with a $2 \times 2 \times 2$ integration scheme. Heat transfer is modeled by assigning the thermal conductivity and heat capacity of the concrete. For the model described in this paper, both the conductivity and heat capacity were modeled as constant.

In the structural analysis, a $3 \times 3 \times 3$ integration scheme is applied by default, but a $2 \times 2 \times 2$ integration scheme can be used in a patch of more than one element to obtain optimal stress points. The stress and strain distribution is approximated over the volume of the element. Stress σ_{xx} and strain ε_{xx} vary linearly in the x direction and

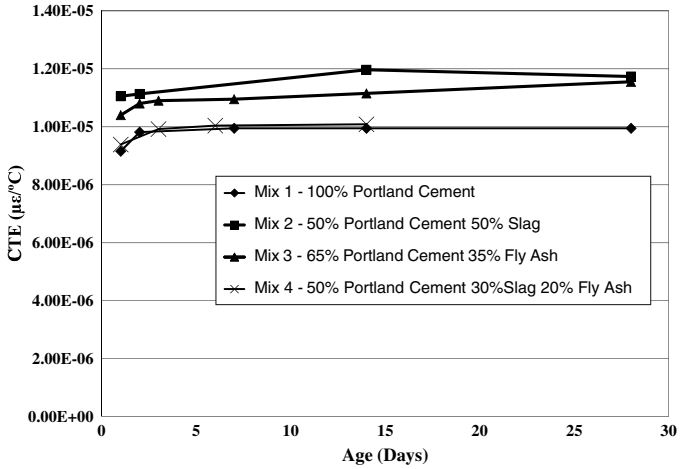

Fig. 9. Coefficient of thermal expansion of concrete mixtures over 28 days

J. Mater. Civ. Eng., 2012, 24(4): 362-372

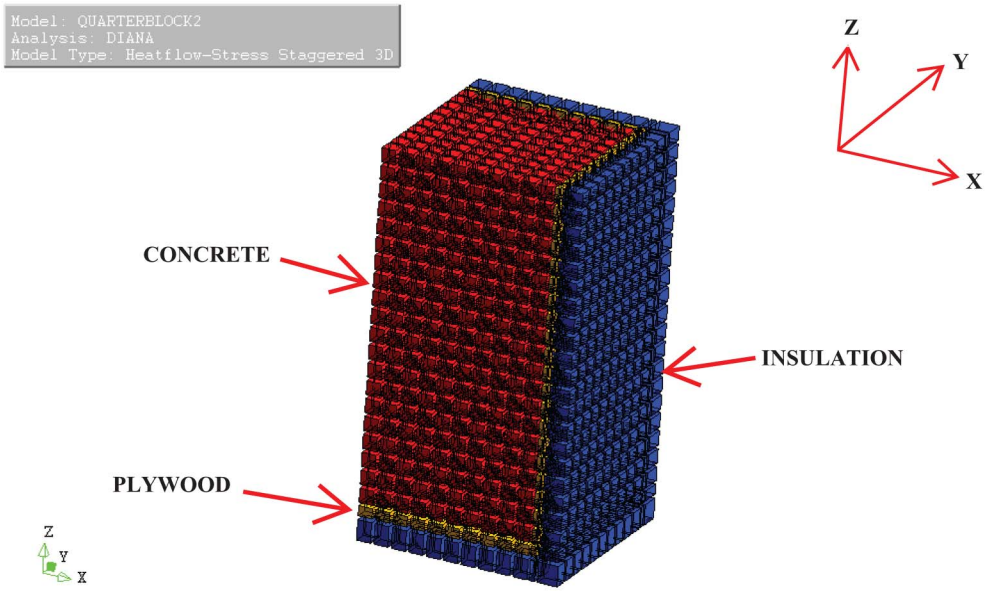

Fig. 10. Finite-element model of one fourth of the concrete block with insulation

quadratically in the y and z directions. Stress σ_{yy} and strain ε_{yy} vary linearly in the y direction and quadratically in the x and z directions. Stress σ_{zz} and strain ε_{zz} vary linearly in the z direction and quadratically in the x and y directions.

The plywood and polystyrene were directly modeled with the three-dimensional eight-node isoparametric brick element, individually using its conductivity and heat capacity to describe the way the heat would be transferred between the concrete, plywood, and polystyrene.

The boundary convection was modeled using a four-node isoparametric quadrilateral element specially used to describe boundaries in three-dimensional thermal analyses. It uses linear interpolation and Gauss integration in its computational scheme. The four nodes in this element were modeled to coincide with the corner nodes of the surface of the brick elements they lie on.

Heat of Hydration

DIANA's preprocessing method for the input of the concrete heat generation function was utilized in this study. The temperature history produced under adiabatic hydration conditions was used as the input and DIANA derives the heat production $q(t)$ from

$$q(t) = c(T, r)\frac{\partial T}{\partial t} \tag{1}$$

where $c(T, r)$ = the capacitance dependent on temperature and degree of reaction r = degree of reaction (percentage of the hydration power used up).

Power data obtained from the isothermal calorimetry testing on cementitious mixtures, shown in Fig. 11, were integrated with respect to time to obtain the energy rise,

$$Q = \int_{t=0}^{t} P\, dt \tag{2}$$

which was then approximated to the energy rise of the hydrating concrete by multiplying by the percent of cementitious content in the concrete mixture it represents. The cementitious content of concrete mixtures used to validate the model are presented in Table 6. The adiabatic temperature rise, presented in Fig. 12, is calculated from the energy using the relationship described by the first law of thermodynamics and expressed in Eq. (3).

$$\Delta Q = m \cdot C_p \cdot \Delta T \quad \text{or} \quad \Delta T = \frac{\Delta Q}{m \cdot C_p} \tag{3}$$

where ΔQ = energy rise (J), m = mass of concrete (g), C_p = specific heat capacity ($J/g - °C$), and ΔT = the change in temperature or temperature rise (°C).

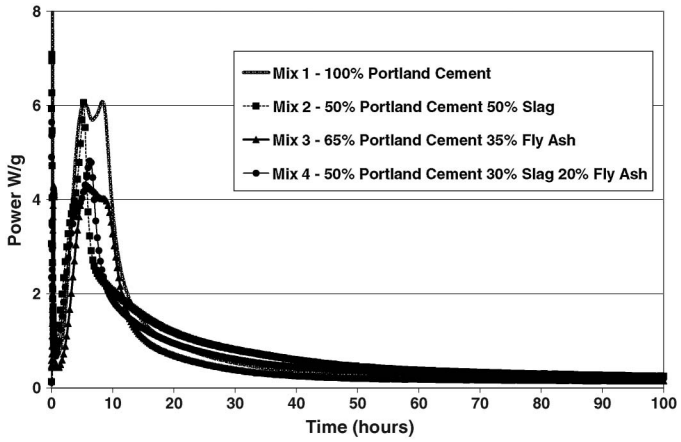

Fig. 11. Hydration power of each cementitious mixture obtained from isothermal calorimetry

Boundary Conditions

The boundary conditions imposed for the thermal analysis consisted of an initial temperature of the model and the external temperature. Both temperatures were set at the temperatures recorded inside the laboratory on the day each concrete mix was made. Fig. 13 presents the temperature history of the laboratory during the monitoring of the experimental blocks. The average temperature of the laboratory for

Table 6. Cementitious Content of each Mixture

Mixture No.	1	2	3	4
Percentage of mixture that is cementitious paste by weight	27.10%	27.10%	27.50%	27.50%

J. Mater. Civ. Eng., 2012, 24(4): 362-372

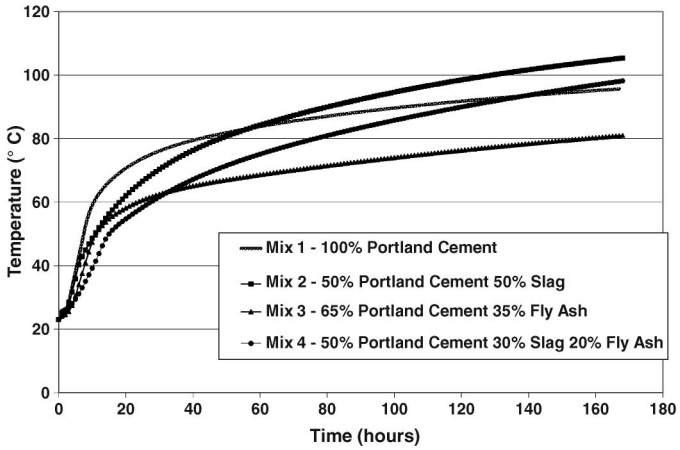

Fig. 12. Adiabatic temperature rise of each concrete mixture calculated from the hydration power obtained in the isothermal calorimetry testing of cementitious mixtures

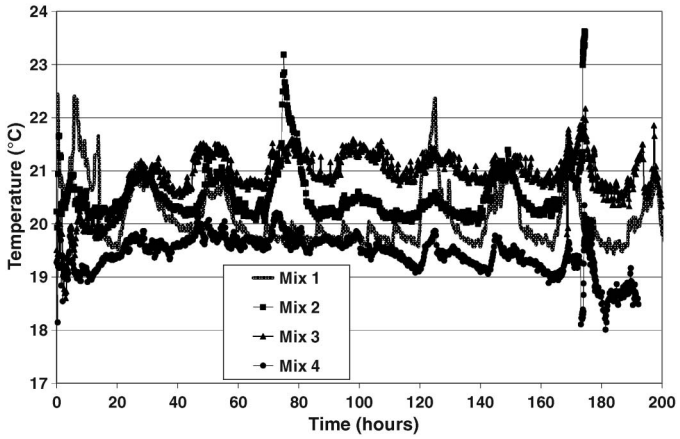

Fig. 13. Average ambient temperatures during experimental block monitoring

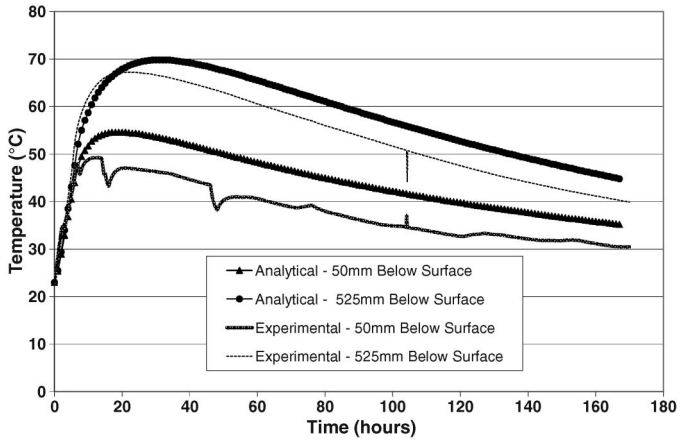

Fig. 14. Isothermal and experimentally measured temperature-time histories below the exposed top surface of mixture 1

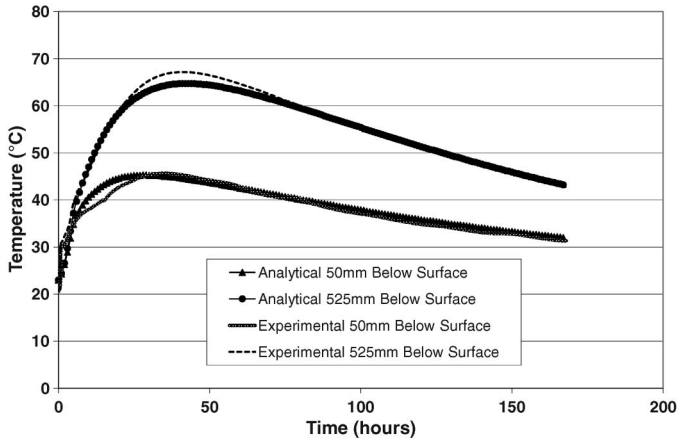

Fig. 15. Isothermal and experimentally measured temperature-time histories below the exposed top surface of mixture 2

blocks 1, 2, and 3, which were cast during the summer months of July and August, was approximately 21°C, whereas for block 4, which was cast in October, it was 20°C.

The boundary conditions imposed for the structural analysis of the quarter block consisted of the restriction of displacements along the symmetry planes; that is, movement of the nodes along the x and y planes of symmetry were restricted in the x and y directions, respectively. The base of the block was modeled as being in a fixed support condition; therefore, displacements along the z direction were also restricted.

Thermal Results

The temperatures obtained in the finite-element analysis of the concrete blocks were compared with the experimentally measured temperatures. Points 50 mm and 525 mm below the top surface along the centerline of the block were chosen for the analysis. These locations were chosen because various Department of Transportation specifications for mass concrete generally limit the temperature differential, measured between temperature sensors, between the midpoint and a point 50 mm inside the exposed face.

The temperature-time histories at locations below the top surface of mixture 1 produced by the finite-element model and measured in the experimental block are presented in Fig. 14. At 50 mm below the surface, the slopes of the profile lines depicting the temperature increase recorded experimentally and analytically are almost identical; however, the predicted peak temperature in the model was 55°C whereas the experimentally measured peak temperature was 49°C. The dips in the experimental block's temperature represent each time the plastic cover placed over the block (to prevent evaporation of the surface water) was lifted off to place the sensors used by a crack monitoring acoustic emission apparatus (the data are not presented in this paper). This affected the peak temperature of points close to the top surface of the block. At 525 mm below the top surface, the effect of the removal of the plastic cover is negligible, and the peak temperature of 69°C calculated in the finite-element model was only 2°C greater than the 67°C measured experimentally.

The trend of the temperature increases obtained from the model of the block with mixtures 2, 3, and 4 are shown in Figs. 15–17. The peak temperatures obtained at 50 mm and 525 mm were all within 2°C of the peak temperatures measured in the experimental block. The similar decreasing trends for each provided enough comfort to conclude that the temperature gradients within the blocks were properly modeled.

Temperature Difference and Cracking

As previously stated, the requirements for the control of heat generation and in particular the maximum allowable temperature difference in mass concrete vary on a state-by-state basis. Currently,

J. Mater. Civ. Eng., 2012, 24(4): 362-372

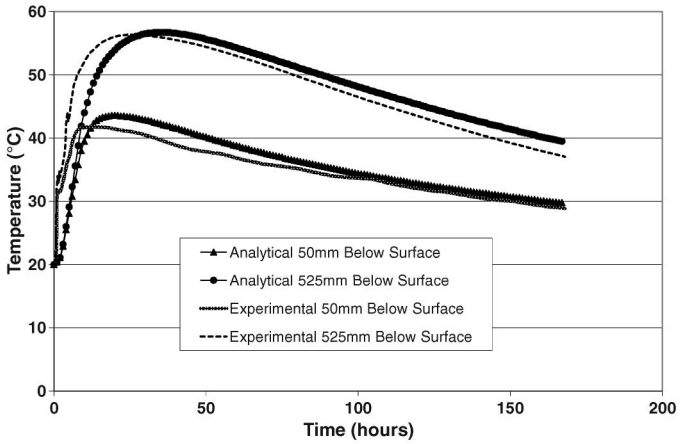

Fig. 16. Isothermal and experimentally measured temperature-time histories below the exposed top surface of mixture 3

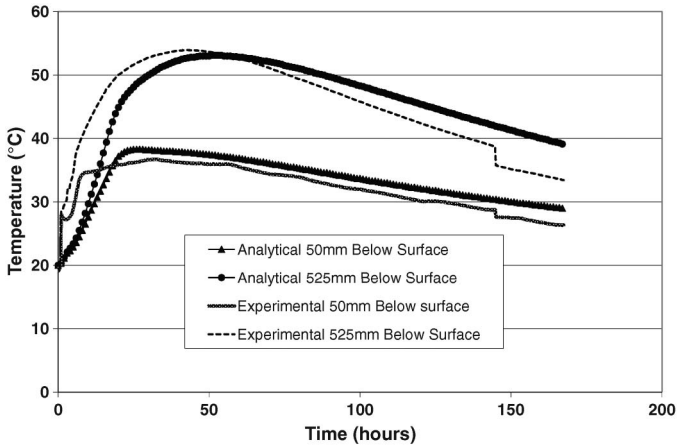

Fig. 17. Isothermal and experimentally measured temperature-time histories below the exposed top surface of mixture 4

no agreement exists on what should be the maximum allowable temperature differential between the center of a mass concrete element and its surface to reduce the occurrence of thermal cracking. The critical temperature differences for the mixtures used in this project are determined from the results of the finite-element analyses on each block.

Fig. 18 shows the plot of the temperature difference between the center and surface of the block with mixture 1. The calculated tensile stresses at the surface exceeded the early age tensile strength value of 1.25 MPa at a temperature differential of 17°C.

Cracking in mixture 2, which contained ground granulated blast-furnace slag, occurred when the temperature differential reached approximately 3°C, as shown in Fig. 19. This is significantly less than the differential in mixture 1, which shows that although the addition of slag to Portland cement slowed the rate of temperature rise, it also caused the concrete to have a lower early age tensile strength of 0.255 MPa, which was to the detriment of the integrity of the structure.

The temperature differential of 8°C at which cracking initiated in mixture 3, shown in Fig. 20, was larger than the differential in mixture 2. In this case, although the fly ash lowered the peak temperature of the concrete, it did not have any effect on rate of initial temperature rise; therefore, a low value of the tensile strength caused the concrete to crack at a lower temperature differential than the block with mixture 1.

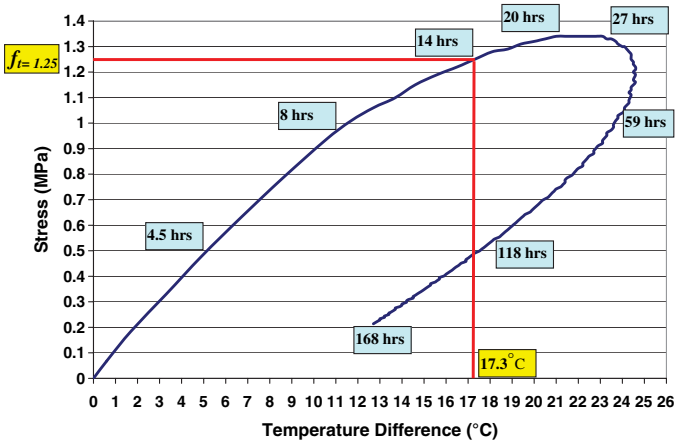

Fig. 18. Time path of induced stress with respect to temperature differential for mixture 1

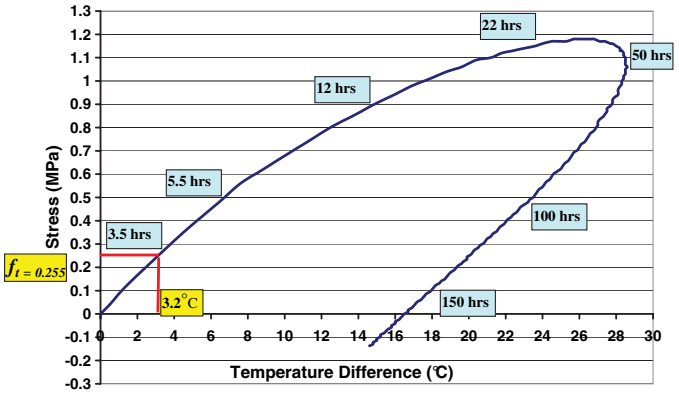

Fig. 19. Time path of induced stress with respect to temperature differential for mixture 2

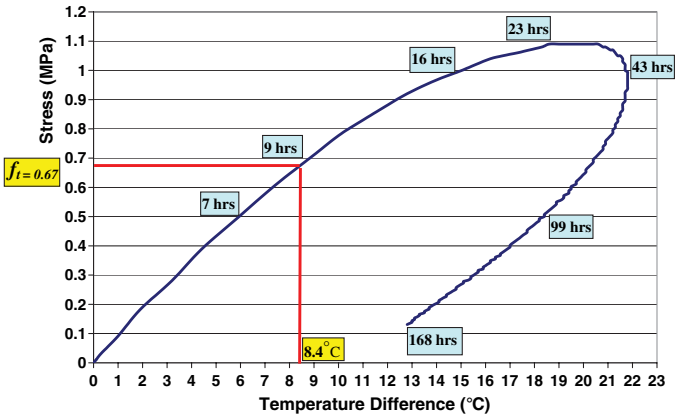

Fig. 20. Time path of induced stress with respect to temperature differential for mixture 3

Fig. 21 shows the plot of the relationship between the temperature difference and induced stress at the surface of the block with mixture 4, and the induced stress is shown to reach the 24 h (day 1) tensile strength of 0.393 MPa when the temperature differential is 21°C, 26 h after being placed.

The results observed in the mixtures containing supplementary cementitious materials are consistent with other research (Bamforth 1984) findings. The formwork was removed on the seventh day

J. Mater. Civ. Eng., 2012, 24(4): 362-372

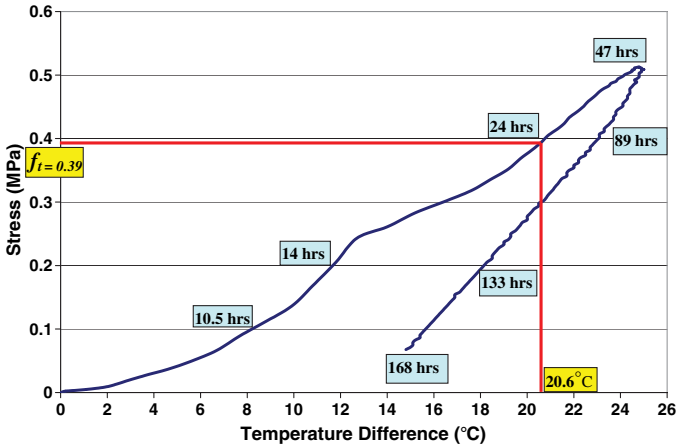

Fig. 21. Time path of induced stress with respect to temperature differential for mixture 4

Fig. 22. Typical location and distribution of cracking found in experimental blocks (image by Adrian M. Lawrence)

after the each concrete mixture was placed. An inspection of each block revealed that thermal cracking did in fact occur during the period of study. The typical crack location and distribution is shown in Fig. 22.

Discussion

The results from the analysis of a finite-element model built to predict the early age behavior of a hydrating concrete element in an effort to quantify the maximum allowable temperature difference to prevent cracking have been presented and discussed. To validate the accuracy of the model and verify the results obtained from the model, four different concrete mixtures were used in experimental blocks with dimensions 1.07 m × 1.07 m × 1.07 m and monitored for temperature distributions. The material and physical properties of the concretes used were obtained from laboratory testing and applied in the finite-element model. Isothermal calorimetry tests were done on the concrete mixtures to determine the energy released during hydration. The calculated adiabatic energy rise obtained from the tests was used as inputs for the model and the predicted temperatures were compared with the temperatures measured in the experimental block. The temperature distributions produced by the model were very similar to those measured in the experimental blocks. The study only focused on the attained tensile strength of concrete specimens at ages greater than one day because current FDOT specifications do not permit the removal of formwork from massive concrete structures that are less than three days of age. The results of the structural analysis for the concrete block study led to the following observations:

- Concrete containing 100% Portland cement experienced tensile stresses high enough to cause cracking on all surfaces, even those insulated, when the temperature difference was 17.3°C.
- In the case for which 50% of the Portland cement was replaced with ground granulated blast-furnace slag, the rate of hydration reaction and the rate of temperature increase was significantly slower. The associated reduction in early age tensile strength resulted in the cracking risk not being reduced.
- The case for which 35% of the Portland cement was substituted with fly ash had, little effect on the early age rate of hydration; thus, the time in which the maximum temperature was achieved was not affected significantly. However, the maximum temperature achieved was itself significantly less. Again, the early age tensile strength was less than the 100% Portland cement case, resulting in similar cracking on all surfaces as before, even though the tensile stresses experienced were less.
- Concrete with a blend of 50% Portland cement, 30% slag, and 20% fly ash performed the best in terms of reducing the induced thermal stresses relative to the tensile strength and, hence, the cracking potential.
- The temperature differential that induced cracking in the concretes used in this project varied from mixture to mixture. This was the result of the corresponding changes in the tensile strength.
- Each of the large-scale block specimens were tested under laboratory conditions; therefore, considering finite-element modeling is necessary for massive concrete structures and elements until modeling becomes more robust and the effect that variation in boundary conditions have on mass concrete are properly quantified.

Conclusions

Reliance on a limiting maximum temperature differential to control cracking in massive concrete applications should be supplemented with a requirement that an analytical method such as finite-element analysis, finite difference, or other analytical limiting calculations that may show that the calculated stress response to the predicted temperature distribution within the concrete will not exceed the tensile strength of the concrete.

The current restrictions on maximum temperature imposed by state regulating bodies should take into consideration the type of cementitious materials that will be used in the concrete mix.

Disclaimer

The views and opinions presented in this document may not represent the official views of State of Florida, the Florida Department of Transportation, or the University of Florida.

Acknowledgments

The authors would like to acknowledge the tremendous efforts put forward by those who contributed to this project. The study was made possible by funding provided by the Florida Department of Transportation. The authors thank Mr. Charles Ishee and Mr. Mario Paredes for their assistance and use of FDOT facilities.

J. Mater. Civ. Eng., 2012, 24(4): 362-372

References

American Concrete Institute (ACI) Committee 207, 207.1R-05. (2005). *Guide to mass concrete*, Farmington Hill, MI.

American Concrete Institute (ACI) Committee 207, 207.2R-07. (2007). *Rep. on thermal and volume change effects on cracking of mass concrete*, Farmington Hills, MI.

Ayotte, E., Massicotte, B., Houde, J., and Gocevski, V. (1997). "Modeling of thermal stresses at early ages in a concrete monolith." *ACI Mater. J.*, 94(6), 577–587.

Ballim, Y. A. (2004). "A numerical model and associated calorimeter for predicting temperature profiles in mass concrete." *Cem. Concr. Compos.*, 26(6), 695–703.

Bamforth, P. B. (1984). "Mass concrete." *Concrete Society digest*, The Concrete Society, London.

De Schutter, G. (2002). "Finite element simulation of thermal cracking in massive hardening concrete elements using degree of hydration based material laws." *Comput. Struct.*, 80(27–30), 2035–2042.

DIANA: Displacement Analyzer Version 9.3 [Computer software]. TNO DIANA BV, Delft, Netherlands.

Evju, C. (2003). "Initial hydration of cementitious systems using a simple isothermal calorimeter and dynamic correction." *J. Therm. Anal. Calorim.*, 71(3), 829–840.

Faria, R., Azenha, M., and Figueiras, J. (2006). "Modeling of concrete at early ages: Application to an externally restrained slab." *Cem. Concr. Compos.*, 28(6), 572–585.

Ferraro, C. C. (2009). "Determination of test methods for the prediction of the behavior of mass concrete." Ph.D. dissertation, Univ. of FL, Gainesville, FL.

Florida Dept. of Transportation (FDOT). (2007). "Standard specifications for road and bridge construction." Tallahassee, FL.

Radovanovic, S. (1998). "Thermal and structural finite element analysis of early age mass concrete structures." Masters thesis, Univ. of Manitoba, Winnipeg, Manitoba, Canada.

Tia, M., Lawrence, A., Ferraro, C., Smith, S., Ochiai, E. (2009). "Development of design parameters for mass concrete using finite element analysis." *Final Rep.*, Dept. of Civil and Coastal Engineering, Univ. of FL, Gainesville, FL.

J. Mater. Civ. Eng., 2012, 24(4): 362-372